Passive Detection of Low-Altitude Signal Sources Using an Improved Cross-Correlation Algorithm

Conghui Cao, Hua Yang, Hao Zhang, Yan Wang and Thomas Aaron Gulliver

November 2018

applied sciences

MDPI

Article

Passive Detection of Low-Altitude Signal Sources Using an Improved Cross-Correlation Algorithm

Conghui Cao [1], Hua Yang [1,*], Hao Zhang [1,2], Yan Wang [1] and Thomas Aaron Gulliver [2]

[1] College of Information Science and Engineering, Ocean University of China, Qingdao 266100, China; shanxilaojia2008@163.com (C.C.); zhanghao@ouc.edu.cn (H.Z.); joko365@163.com (Y.W.)

[2] Department of Electrical and Computer Engineering, University of Victoria, Victoria, BC V8W 2Y2, Canada; agullive@ece.uvic.ca

* Correspondence: hyang@ouc.edu.cn; Tel.: +86-186-6176-6035

Received: 11 October 2018; Accepted: 19 November 2018; Published: 22 November 2018

Abstract: The passive detection of low-altitude signal sources is studied using an improved cross-correlation method in the time–frequency domain. A matching template is designed for signal cross-correlation, and a cross-correlation threshold is used to determine whether a signal source is present or not. An improved cross-correlation method is also proposed to estimate the direction of arrival and communication frequency of a signal source. Furthermore, the distance and signal-to-noise ratio are estimated using an energy detector. Outdoor data from a bridge in the Jimo District, Qingdao, and indoor data from a research laboratory are used for performance evaluation. The results obtained show that the proposed method can provide better passive detection of low-altitude signal sources compared to several well-known algorithms in the literature. In addition, this method is more suitable for long-distance detection.

Keywords: signal detection; low-altitude signal source; unmanned aerial vehicle (UAV); cross-correlation; time–frequency analysis

1. Introduction

The detection and management of low-altitude signal sources have recently attracted significant research interest [1]. An unmanned aerial vehicle (UAV) is a typical low-altitude signal source which communicates with a controller using radio frequency (RF) signals [2]. According to a Consumer Electronics Association (CEA) survey, global sales of UAVs reached 69 million in 2015 and may exceed 1 billion by 2020. In addition, UAV costs are decreasing, while the number of applications is increasing [3–6]. Civilian UAVs have become widespread and are now affecting air traffic, disrupting operations, and violating privacy laws [7]. Many techniques have been proposed to detect aerial targets including laser scanners, acoustic detectors, infrared thermal cameras, and visual observations. Acoustic detection is only effective over short distances of 300 m or less [2]. Distinguishing different low-altitude signal sources beyond 1.5 km is difficult using infrared thermal cameras and visual observations [8]. A laser scanner transmits a pulse signal and measures the propagation time, so active target detection is employed [9]. Thus, these techniques are not suitable for passive detection of low-altitude signal sources at distances up to 3 km. This motivates the development of new methods in this paper.

Passive radar can be used to detect signal sources by sensing the corresponding RF signals [10]. Linear fusion has been employed previously [11] for target recognition in a passive multistatic radar system, and bistatic range measurements have been used to find the position of a target [12]. In [13], the location of a continuous wave signal source was estimated passively using the phase variance. Passive estimation of the position of a high-altitude aircraft was achieved in [14] using a satellite signal.

The detection of moving targets in multipath environments with a passive radar was studied in [15]. In [16], the location of a target was obtained using a passive coherent method with the help of an illuminator. These approaches were employed only for ground and high-altitude target detection and most require the assistance of a satellite or mobile transmitter. The passive detection of RF signals from low-altitude signal sources has not been adequately investigated, particularly when auxiliary information or transmitters are not available. Thus, in this paper, the RF communication signals from a target such as a UAV are considered for the passive detection of low-altitude sources.

Cross-correlation is a common signal detection method in radar systems and has been employed in both the frequency and time domains [17–20]. In [17], a Gaussian mixture model was proposed to sense double-talk using cross-correlation in the frequency domain. Cross-correlation and a finite state machine were employed in [18] to detect vehicles parked indoors. In [19], an algorithm for phase offset estimation was developed using the Hilbert transform and signal cross-correlation. Cross-correlation has also been used for seismic monitoring [20]. In this paper, cross-correlation in the time–frequency domain is employed for the passive detection of low-altitude signal sources.

Several parameters can be estimated for a signal source, such as the direction of arrival (DOA), frequency range, signal-to-noise ratio (SNR), and the distance between the source and receiver [21–25]. A DOA estimation algorithm for low-altitude targets was proposed in [21] which employs a microphone array [21]. In [22], adaptive frequency estimation was implemented using a data-selection strategy. The SNR was obtained when the useful signal occupies a separate range in the frequency domain and all other components are clutter [23]. In [24], the distance was estimated using the received signal strength indicator (RSSI). Parameter estimation for low-altitude signal sources is considered here.

In this paper, an improved cross-correlation method for the passive detection of low-altitude signal sources is proposed. The contributions are as follows.

(1) Communication signals from low-altitude signal sources are collected in real-world outdoor and indoor environments for the first time.
(2) The signals are analyzed in the time–frequency domain, and a cross-correlation threshold method is proposed to distinguish whether a signal source is present or not.
(3) An improved cross-correlation method is proposed to estimate the DOA and communication frequency of a low-altitude signal source.
(4) The proposed method is compared with several well-known techniques in the literature. The results obtained show that this method provides better detection of low-altitude signal sources, particularly over long distances.

The remainder of this paper is organized as follows. The low-altitude signal source system model and the noise reduction algorithm are presented in Section 2. The cross-correlation threshold classification method and parameter estimation for a low-altitude signal source are presented in Section 3. In Section 4, the performance of the proposed algorithm is evaluated using real-world outdoor and indoor data. Finally, some concluding remarks are given in Section 5.

2. System Model

The communication signals between a controller and a low-altitude source can be used for passive detection. In general, they consist of several fixed carrier signals. The system model includes a signal source u, a controller c, and a passive receiver Rx, as shown in Figure 1. The dashed lines indicate that the receiver collects the signals passively, while the solid line represents the active communications between the source and controller. A line-of-sight (LOS) channel is assumed between the source and receiver, and a non-line-of-sight (NLOS) channel between the controller and receiver [2]. A UAV is considered in this paper as a typical low-altitude signal source. A UAV communicates with the corresponding controller in the frequency range 2.4 GHz to 2.5 GHz using orthogonal frequency division multiplexing (OFDM) and frequency hopping (FH).

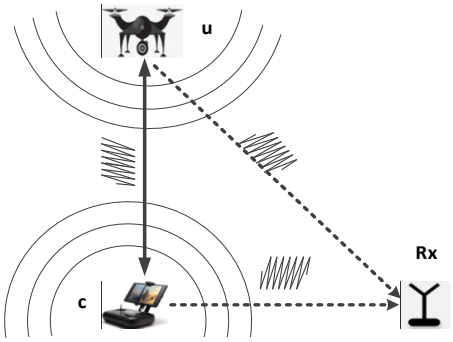

Figure 1. The system model which includes a signal source u, a controller c, and a passive receiver Rx. The dashed lines indicate that the receiver collects the signals passively, while the solid line represents the active communications between the source and controller.

The Phantom 4 Pro UAV from DJ-Innovations was employed in the experiments. One experiment was carried out outdoors with the Rx placed on a bridge in the Jimo District, Qingdao, Shandong Province, China, with the UAV moving away from the Rx at distances of 500 m, 1000 m, 1500 m, 2000 m, 2500 m, and 3000 m, as shown in Figure 2a. The UAV hovered at a height of 100 m in the outdoor test. Another experiment was conducted indoors in a research laboratory with the Rx on a table 1.1 m above ground and the UAV on another table at distances of 5 m and 10 m from the Rx, as shown in Figure 2b. The antenna gain is 24 dBi, the beam width is 10°, and the frequency range is 2.3 GHz to 2.7 GHz. During the experiments, the antenna elevation angle was varied from 0° to 12° and the azimuth angle from 0° to 180°. The same parameters were used in the experiments with multiple UAVs.

(**a**) (**b**)

Figure 2. The test environments (**a**) outdoors and (**b**) indoors.

The detection environment contains static and nonstatic clutter as well as Gaussian noise. The discrete frequency domain signal received from the antenna is $X(\omega)$ with length N = 5120. The corresponding time domain signal can be obtained using an inverse discrete Fourier transform (IDFT), which gives

$$x(n) = \frac{1}{N}\sum_{\omega=0}^{N-1} X(\omega)e^{\frac{i2\pi n\omega}{N}}, n = 0, 1, \ldots, N-1 \quad (1)$$

This includes the UAV signal, nonstatic clutter, additive white Gaussian noise (AWGN), and static clutter such as Bluetooth and WiFi signals. The autocorrelation of this signal is

$$r(n, n') = x^*(n - n'/2)x(n + n'/2) \quad (2)$$

where n' is the time delay and $(\cdot)^*$ denotes conjugate. In order to observe the time and frequency domain features of the UAV signal simultaneously [26], the Wigner–Ville distribution (WVD) of $x(n)$ can be expressed as

$$y_{n\omega} = \sum_{n'=-(N-n-1)/2}^{(N-n-1)/2} r(n,n') e^{\frac{-i2\pi n'\omega}{N}} \tag{3}$$

where n denotes time, ω denotes frequency, and $y_{n\omega}$ denotes the power at frequency ω and time n.

The passive receiver rotates from 0° to 180° with a rotation speed of 22.5°/s, so the antenna rotates 180° in 8 s. The time sampling interval is t_a = 0.02 s, the frequency range is 2.4 GHz to 2.5 GHz, and the frequency sampling interval is f_w = 19.53 kHz. The discrete time–frequency values are then $y_{jk}, j = 1,\ldots,8/t_a, k = 1,\ldots,(2.5-2.4)\times 10^9/f_w$. y_{jk} is the power at frequency $kf_w + 2.4\times 10^9$ and time jt_a. These values in an ideal environment are shown in Figure 3a with the UAV at a relative angle of 97.88° and a distance of 1.5 km from the Rx. Figure 3b shows the time–frequency matrix received in a real-world environment with the UAV in the same position. Linear spatial filtering is commonly employed for image enhancement and noise reduction and so is used here by considering a matrix as an image [27]. This involves convolution using a sliding filter template w with dimensions $M \times O$, which gives

$$\hat{y}_{jk} = w * \begin{bmatrix} y_{jk} & \cdots & y_{j(k+O-1)} \\ \vdots & \ddots & \vdots \\ y_{(j+M-1)k} & \cdots & y_{(j+M-1)(k+O-1)} \end{bmatrix} \tag{4}$$

where $w = [w_1,\ldots,w_o,\ldots,w_O]$, $w_o = [w_{1o},\ldots,w_{Mo}]^H$, H denotes the transpose, $*$ denotes convolution, and $w = \begin{bmatrix} 0.0302 & 0.0446 & 0.591 & 0.0735 & 0.0345 \\ 0.0543 & 0.0399 & 0.0254 & 0.0110 & 0 \\ 0 & 0 & 0 & 0 & 0 \end{bmatrix}$. The time–frequency matrix is normalized so that

$$\dot{y}_{jk} = \frac{\hat{y}_{jk} - \hat{y}_{\min}}{\hat{y}_{\max} - \hat{y}_{\min}} \tag{5}$$

where $\hat{y}_{\max}$ and $\hat{y}_{\min}$ are the maximum and minimum values of the matrix, and $\hat{y}_{jk}, j = 1,\ldots,8/t_a, k = 1,\ldots,(2.5-2.4)\times 10^9/f_w$. The time–frequency matrix after filtering and normalization is shown in Figure 3c. This indicates that the signal consists of several carriers with a bandwidth of 9.47 MHz between 3.8 s and 4.9 s. The time–frequency matrix in a real-world environment with no UAV is shown in Figure 3d for comparison.

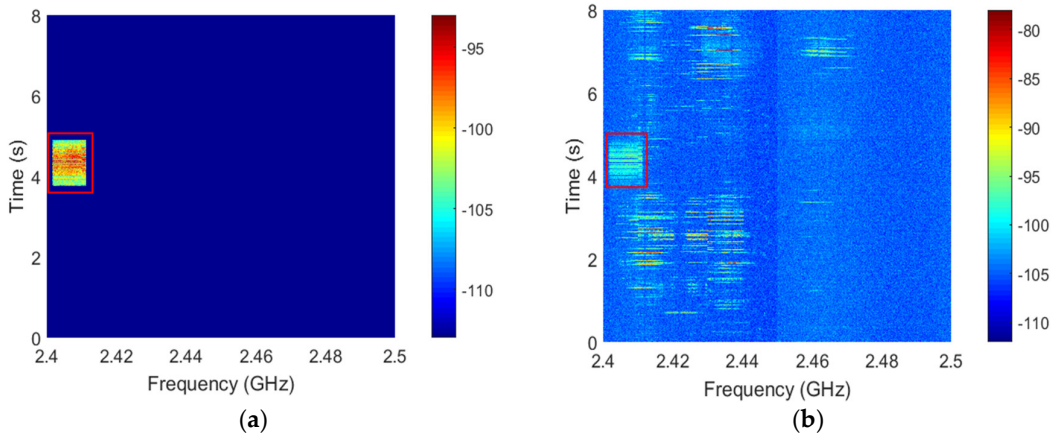

Figure 3. *Cont.*

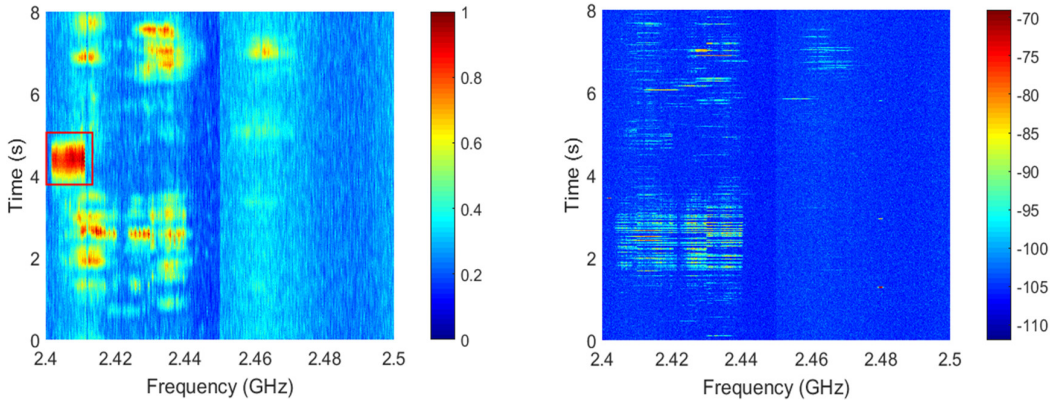

Figure 3. (**a**) The time–frequency matrix in an ideal environment with the unmanned aerial vehicle (UAV) present, (**b**) the matrix in a real-world environment with the UAV present, (**c**) the matrix after filtering and normalization in a real-world environment with the UAV present, and (**d**) the matrix in a real-world environment with no UAV present.

3. Proposed Algorithm

In this section, a cross-correlation threshold method is employed for the detection of a low-altitude signal source. An improved cross-correlation algorithm is proposed to estimate the frequency and DOA. In addition, the SNR and distance estimation are also discussed.

3.1. Low-Altitude Signal Source Detection

The similarity of two signals can be evaluated using the cross-correlation [19]. The original signal received at time jt_a is shown in Figure 4a. In order to detect a low-altitude signal source, a matching template is designed to calculate the cross-correlation with the received signal. This template is shown in Figure 4b and is given by $m = [m_1, \ldots, m_L]$, $L = 10.645\ \text{MHz}/f_w$. The cross-correlation using the proposed template and other templates using wavelet shapes such as the Daubechies, Morlet, and Mexican Hat templates are shown in Figure 4c. This shows that the proposed template provides the best performance. At time jt_a, the forward cross-correlation between the sliding template and the received signal can be expressed as

$$\dot{R}_{jk} = \begin{cases} \dfrac{\sum_{i=1}^{L}(m_i-\overline{m})\left(\dot{y}_{j(k+i-1)}-\overline{v}\right)}{\sqrt{\sum_{i=1}^{L}(m_i-\overline{m})^2}\sqrt{\sum_{i=1}^{L}\left(\dot{y}_{j(k+i-1)}-\overline{v}\right)^2}}, & k = 1,2,\ldots,(2.5-2.4)\times 10^9/f_w - L \\ 0, & k = (2.5-2.4)\times 10^9/f_w - L + 1,\ldots,(2.5-2.4)\times 10^9/f_w \end{cases} \quad (6)$$

where k is the kth sliding position at time jt_a; $k = 1, 2, \ldots, (2.5{-}2.4) \times 10^9/f_w - L + 1$, $j = 1, \ldots, 8/t_a$, L is the length of the template, $\dot{y}_{j(k+i-1)}$ is the power at frequency $(k+i-1)f_w + 2.4 \times 10^9$ and time jt_a, $v = \left[\dot{y}_{jk}, \ldots, \dot{y}_{j(k+L-1)}\right]$, $\overline{v}$ is the mean of the vector v, $\overline{m}$ is the mean of the template m, and $\dot{R}_{jk}$ is the kth cross-correlation coefficient at time jt_a.

In order to determine whether a UAV is present or not at time jt_a, an improved cross-correlation threshold method is used which is given by

$$\dot{R}_j = \max(\dot{R}_{jk}),\ k = 1,2,\ldots,(2.5-2.4)\times 10^9/f_w \quad (7)$$

The cross-correlation threshold is set to 0.7 so $\dot{R}_j$ exceeding this value indicates that a UAV is present.

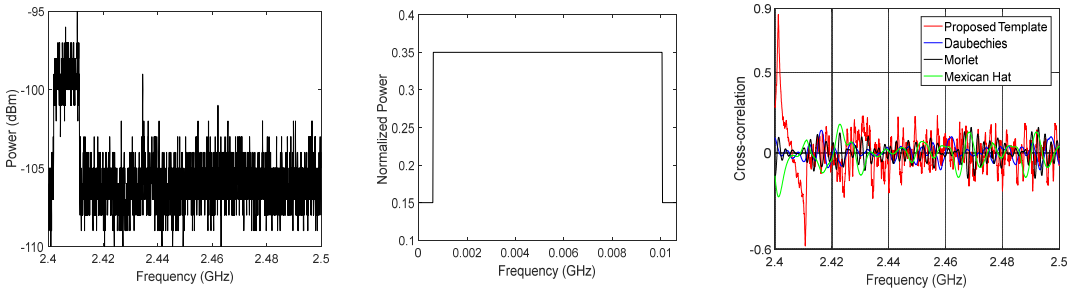

(**a**) (**b**) (**c**)

Figure 4. (**a**) The received signal at time jt_a, (**b**) the matching template, and (**c**) the cross-correlation using different templates.

3.2. Frequency and Direction of Arrival Estimation

When a low-altitude signal source is present, the frequency of the received signal can be estimated using the proposed cross-correlation method. At time jt_a, the backward cross-correlation between the template and received signal is

$$\hat{R}_{jk} = \begin{cases} 0, & k = 1, 2, \ldots, L \\ \dfrac{\sum_{i=1}^{L} (m_i - \overline{m})\left(\dot{y}_{j(k+i-L-1)} - \overline{z}\right)}{\sqrt{\sum_{i=1}^{L} (m_i - \overline{m})^2} \sqrt{\sum_{i=1}^{L} \left(\Gamma y_{j(k+i-L-1)} - \overline{z}\right)^2}}, & k = L+1, \ldots, (2.5-2.4) \times 10^9 / f_w \end{cases} \tag{8}$$

where $\mathrm{z} = \left[\dot{y}_{j(k-L)}, \ldots, \dot{y}_{j(k-1)}\right]$ and $\overline{z}$ is the mean of z. The improved cross-correlation is given by

$$\widetilde{R}_{jk} = \max\left(\dot{R}_{jk}, \hat{R}_{jk}\right) \tag{9}$$

where $\widetilde{R}_{jk}$ is the kth cross-correlation coefficient at time jt_a, the cross-correlation array at time jt_a is $\widetilde{R}_j = [\widetilde{R}_{j1}, \ldots, \widetilde{R}_{jk}, \ldots, \widetilde{R}_{j((2.5-2.4)\times 10^9/f_w)}]$, $k = 1, 2, \ldots, (2.5-2.4) \times 10^9 / f_w$, and the improved cross-correlation matrix in the time–frequency domain is $\widetilde{R} = \left[\widetilde{R}_1, \ldots, \widetilde{R}_j, \ldots, \widetilde{R}_{8/t_a}\right]^H$, $j = 1, \ldots, 8/t_a$.

In order to reduce the cross-correlation value of the clutter signal and enhance the cross-correlation value of the signal source simultaneously, a time–frequency domain accumulation method is employed. The improved cross-correlation matrix after three rounds of accumulation can be expressed as

$$R_{jk} = \sum_{l=1}^{3} \widetilde{R}_{jk}^{l} \tag{10}$$

Figure 5a shows the improved cross-correlation matrix of the signal in Figure 3b after accumulation, and Figure 5b shows the matrix of the signal in Figure 3d after accumulation.

The low-altitude signal shown in Figure 5c has a bandwidth of 9.47 MHz between 2.401758 GHz and 2.411228 GHz. The start of this signal is

$$f_{start} = \begin{cases} K_b f_w + 2.4 \times 10^9 & s.t. (K_{b+1} - K_b) \geq 8 \times 10^6 / f_w, \\ & K_b \in K, K_1 \leq \ldots \leq K_b \leq \ldots \leq K_B, b = 1, \ldots, B, \\ & K = k\Big|_{(\exists\ R_{jk} \geq 0.7)}, \\ & 1 \leq j \leq 8/t_a, \\ & 1 \leq k \leq (2.5-2.4) \times 10^9 / f_w - L + 1, \\ 0 & \text{otherwise} \end{cases} \tag{11}$$

where K is the array of frequency positions that exceed the cross-correlation threshold and B is the length of K. The elements in K are sorted in ascending order. When the difference between adjacent elements exceeds $8 \times 10^6 / f_w$, the start frequency is found, and vice versa. The end position of the frequency range is found in the same way and is given by

$$f_{end} = \begin{cases} K_{b+1} f_w + 2.4 \times 10^9 & s.t. (K_{b+1} - K_b) \geq 8 \times 10^6 / f_w, \\ & \quad K_b \in K, K_1 \leq \ldots \leq K_b \leq \ldots \leq K_B, b = 1, \ldots, B, \\ & \quad K = k\Big|_{(\exists\ R_{jk} \geq 0.7)}, \\ & \quad 1 \leq j \leq 8/t_a, \\ & \quad 1 \leq k \leq (2.5 - 2.4) \times 10^9 / f_w - L + 1, \\ 0 & \text{otherwise} \end{cases} \tag{12}$$

The frequency range is then

$$f_{range} = \begin{cases} f_{end} - f_{start} & s.t. f_{end} \neq 0, \\ & \quad f_{start} \neq 0, \\ 0 & \text{otherwise} \end{cases} \tag{13}$$

From the rotational speed and location of the antenna, the correspondence between the time and direction can be expressed as

$$p = \frac{180t}{8} \tag{14}$$

Note that a directional antenna is employed. The DOA of the low-altitude signal source can be obtained using frequency f_{start} as shown in Figure 5d. The time of the maximum power can be used as an estimate of the time when the source appears which is given by

$$\begin{aligned} & \dot{t} = J t_a \\ & s.t.\ J = j\Big|_{(\forall \max(R_{jk}))}, \\ & \quad 1 \leq j \leq 16/t_a \\ & \quad k = \left(f_{start} - 2.4 \times 10^9\right) / f_w \end{aligned} \tag{15}$$

Thus, the time corresponding to the maximum cross-correlation value at frequency f_{start} is considered to be the start of the source signal. Using (14) and (15), the DOA estimate is

$$\begin{aligned} & \dot{p} = 22.5 J t_a \\ & s.t.\ J = j\Big|_{(\forall \max(R_{jk}))}, \\ & \quad 1 \leq j \leq 8/t_a \\ & \quad k = \left(f_{start} - 2.4 \times 10^9\right) / f_w \end{aligned} \tag{16}$$

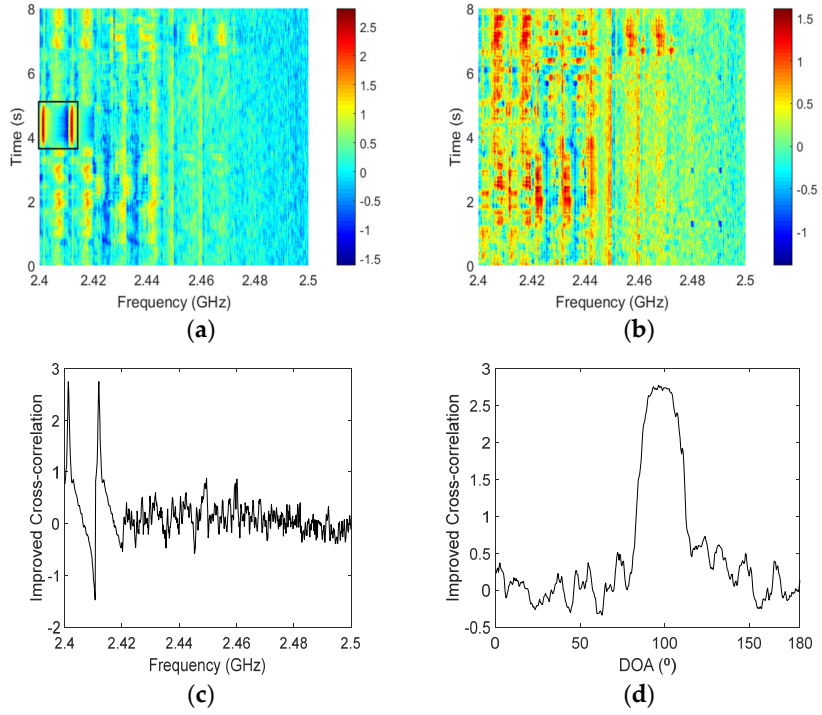

Figure 5. (**a**) The improved cross-correlation using accumulation with the UAV present, (**b**) the improved cross-correlation using accumulation with no UAV present, (**c**) frequency estimation with a UAV present, and (**d**) direction of arrival (DOA) estimation at frequency f_{start}.

3.3. SNR Estimation and Distance Estimation

According to [23], the signal to noise ratio (SNR) can be defined as the ratio of the signal energy at the carrier frequency to the noise energy at this frequency, which can be expressed as

$$\mathrm{SNR} = 20\log_{10}\left(\frac{P_r}{Q_r}\right) \tag{17}$$

where the signal power is

$$P_r = \sum_{k=(f_{start}-2.4\times10^9)/f_w}^{(f_{end}-2.4\times10^9)/f_w} \dot{y}_{(\dot{t}/t_a)k} \tag{18}$$

and the noise power is

$$Q_r = \sum_{k=1}^{(f_{start}-2.4\times10^9)/f_w-1} \dot{y}_{(\dot{t}/t_a)k} + \sum_{k=(f_{end}-2.4\times10^9)/f_w+1}^{(2.5-2.4)\times10^9/f_w} \dot{y}_{(\dot{t}/t_a)k} \tag{19}$$

The RSSI is used to estimate the distance between the receive antenna and signal source, as the signal strength decreases with distance. The fading characteristics of the channel have a log-normal distribution, so the path loss can be expressed as

$$PL(d) = PL(d_0) + 10\times n\times\log_{10}\left(\frac{d}{d_0}\right) + X_\sigma \tag{20}$$

where d is the distance between the source and receiver, n is the path loss index, X_σ is a Gaussian distributed random variable with zero mean and standard deviation σ, and d_0 is the reference distance. The received signal power is then

$$P_r = P_t - PL(d) \tag{21}$$

where P_t is the transmit power and

$$P_0 = P_t - PL(d_0) \tag{22}$$

so that

$$PL(d_0) = P_t - P_0 \tag{23}$$

Using (20) and (23), the path loss at a distance d after averaging multiple measurements is

$$PL(d) = P_t - P_0 + 10 \times n \times \log_{10}\left(\frac{d}{d_0}\right) \tag{24}$$

where X_σ is neglected because the mean of X_σ is 0. Then, from (21) and (24), the received signal strength at a distance d is

$$P_r = P_0 - 10 \times n \times \log_{10}\left(\frac{d}{d_0}\right) \tag{25}$$

so the distance between the receiving antenna and signal source can be estimated as

$$d = d_0 \times 10^{\frac{P_0 - P_r}{10n}} \tag{26}$$

4. Performance Results

The passive detection of low-altitude signal sources is evaluated in this section using the advanced method (AM) [2], and the constant false alarm rate (CFAR) [28], higher-order cumulant (HOC) [29], and proposed methods. For the CFAR algorithm, the two-dimensional (2-D) energy window slides over the entire time–frequency matrix to detect the signal source. This window consists of outer, protected, and inner windows. When the window is aligned with the signal source, the inner window corresponds to the signal source, the outer window corresponds to the noise, and the protected window is the buffer between the outer and the inner windows. Thus, when a signal source is present, the inner window to outer window energy ratio will be high. The width of the inner window is set to 9.47 MHz based on the UAV signal, and the height of this window is set to 0.7 s according to the presence of a UAV. For the HOC method, a window slides over the entire time–frequency matrix. The fourth-order cumulant of the signal covered by the window is used. When a low-altitude signal source is detected, the value of this cumulant is high. The width of the HOC window is set to 9.47 MHz.

4.1. Outdoor Experiments

In this section, the performance of the outdoor passive detection is evaluated for single and multiple low-altitude signal sources. The false alarm probability and missing alarm probability outdoor are determined using the proposed method and advanced method. In addition, outdoor parameter estimation results are given for the proposed, HOC, and CFAR methods.

4.1.1. Outdoor Passive Detection of a Low-Altitude Signal Source

The data was obtained on a bridge in Jimo, Qingdao, in a region with dimensions 1000 m × 4500 m × 200 m. A dataset refers to the data acquired during one rotation of the receive antenna. The normalized time–frequency matrices after filtering are given in Figure 6 for different distances between the UAV and receiver. These results show that the power of the received signal decreases with distance, as expected. In the experiments, the time that the signal source appears, the direction of arrival, and the start frequency used for communication differ depending on the distance. For outdoor distances of 500 m, 1000 m, 1500 m, 2000 m, 2500 m, and 3000 m, the actual directions of arrival are 85.815°, 95.196°, 98.27°, 99.43°, 37.035°, and 37.642°, respectively. The actual start frequencies are 2.401758 GHz, 2.401758 GHz, 2.401758 GHz, 2.401758 GHz, 2.471992 GHz, and 2.471992 GHz for the same distances from 500 m to 3000 m, respectively.

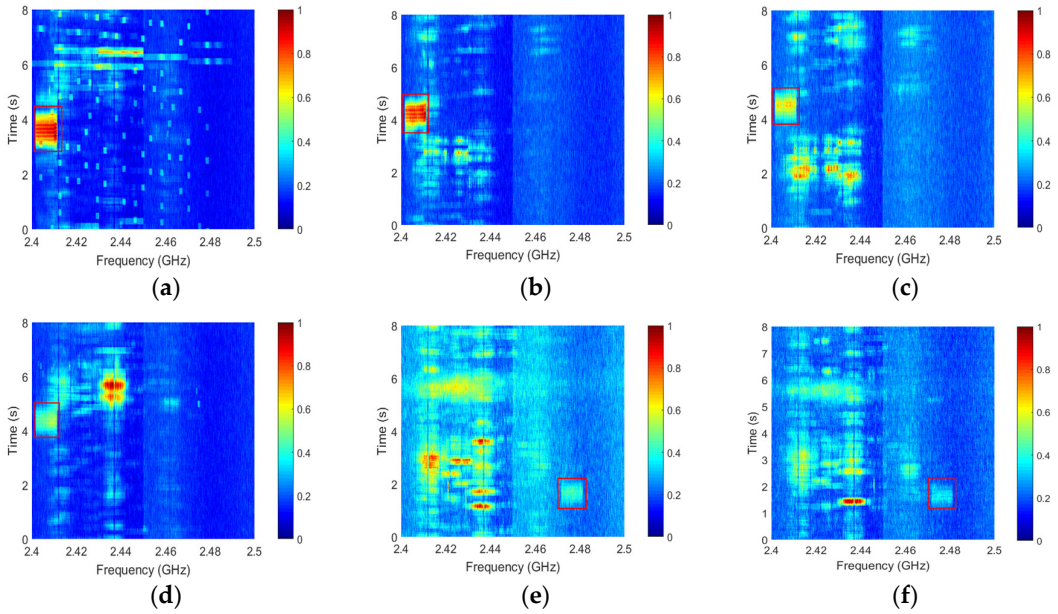

Figure 6. Normalized time–frequency matrices after filtering at outdoor distances of (**a**) 500 m, (**b**) 1000 m, (**c**) 1500 m, (**d**) 2000 m, (**e**) 2500 m, and (**f**) 3000 m.

The false alarm probability refers to the percentage of signals incorrectly classified as a UAV being present. Conversely, the missing alarm probability refers to the percentage of signals incorrectly classified as a UAV not being present. In total, 3000 datasets were obtained from the outdoor experiments. Figure 7 presents the false alarm probability and missing alarm probability for different numbers of datasets and different outdoor distances. This shows that for 1500 datasets, the false alarm probabilities are 0.0678 and 0.0527 for the AM and proposed method, respectively. Figure 7b shows that at a distance of 2000 m, the missing alarm probabilities are 0.1275 and 0.0431 for the AM and proposed method, respectively. The missing alarm probability increases with distance, as expected. These results indicate that the proposed algorithm has better performance than the AM.

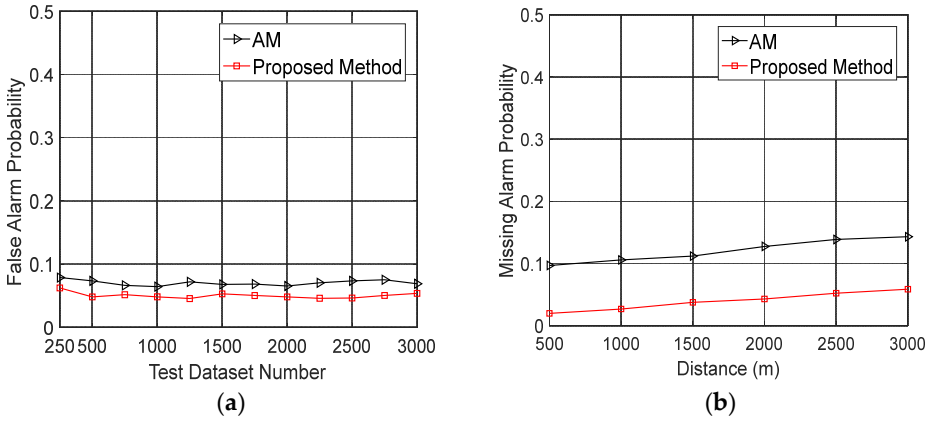

Figure 7. (**a**) The false alarm probability for different numbers of outdoor datasets, and (**b**) the missing alarm probability for different outdoor distances. AM: advanced method.

The results for the improved cross-correlation method at different outdoor distances are given in Figure 8. This shows that the cross-correlation is larger in the target area compared to where there is just noise and clutter. Figures 9 and 10 present the frequency and DOA estimation results for several outdoor distances obtained using the proposed method. The frequency estimates are 2.401776 GHz,

2.401746 GHz, 2.401764 GHz, 2.401782 GHz, 2.471985 GHz, and 2.471981 GHz for increasing distances, and the corresponding DOA estimates are 90.22°, 94.58°, 96.09°, 97.83°, 36.43°, and 38.35°.

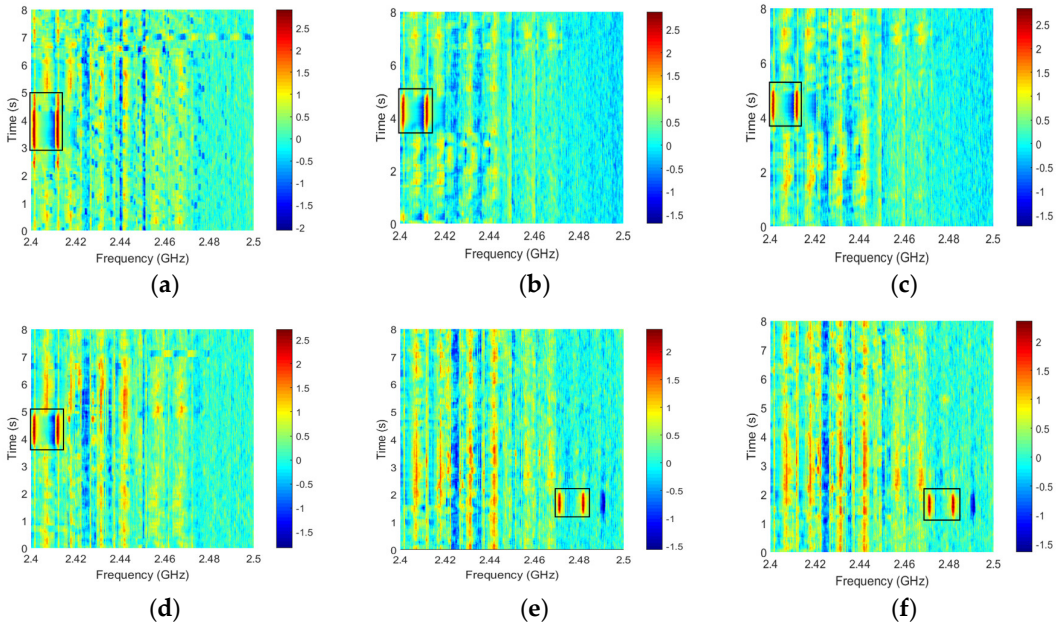

Figure 8. The results for the improved cross-correlation method at outdoor distances of (**a**) 500 m, (**b**) 1000 m, (**c**) 1500 m, (**d**) 2000 m, (**e**) 2500 m, and (**f**) 3000 m.

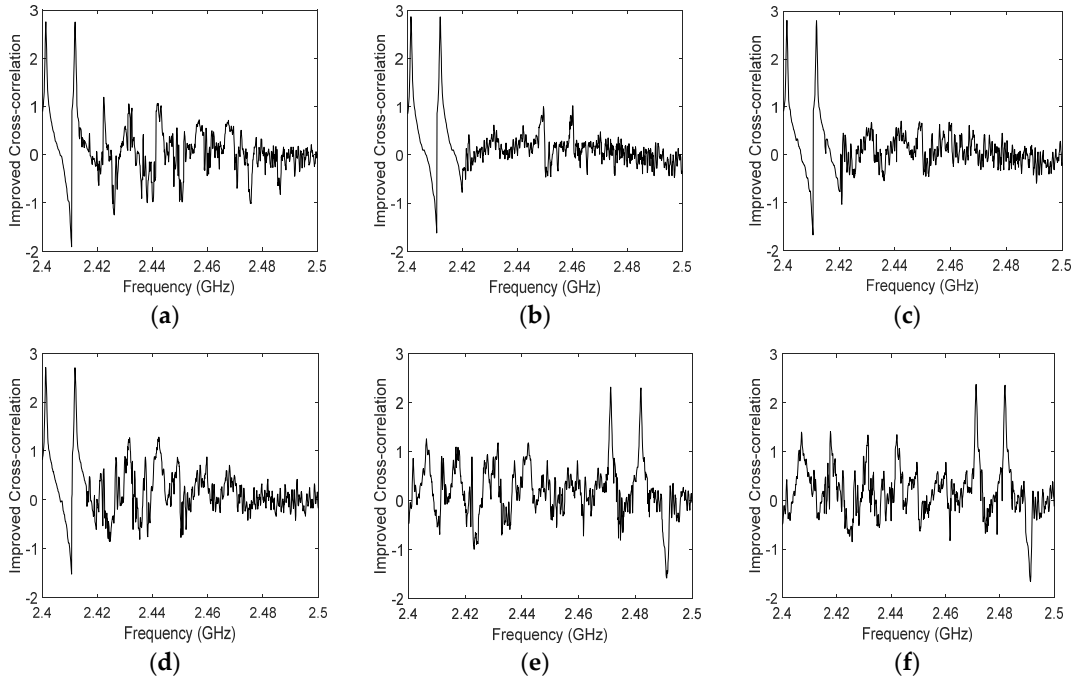

Figure 9. The frequency estimation results using the proposed method outdoors at distances of (**a**) 500 m, (**b**) 1000 m, (**c**) 1500 m, (**d**) 2000 m, (**e**) 2500 m, and (**f**) 3000 m.

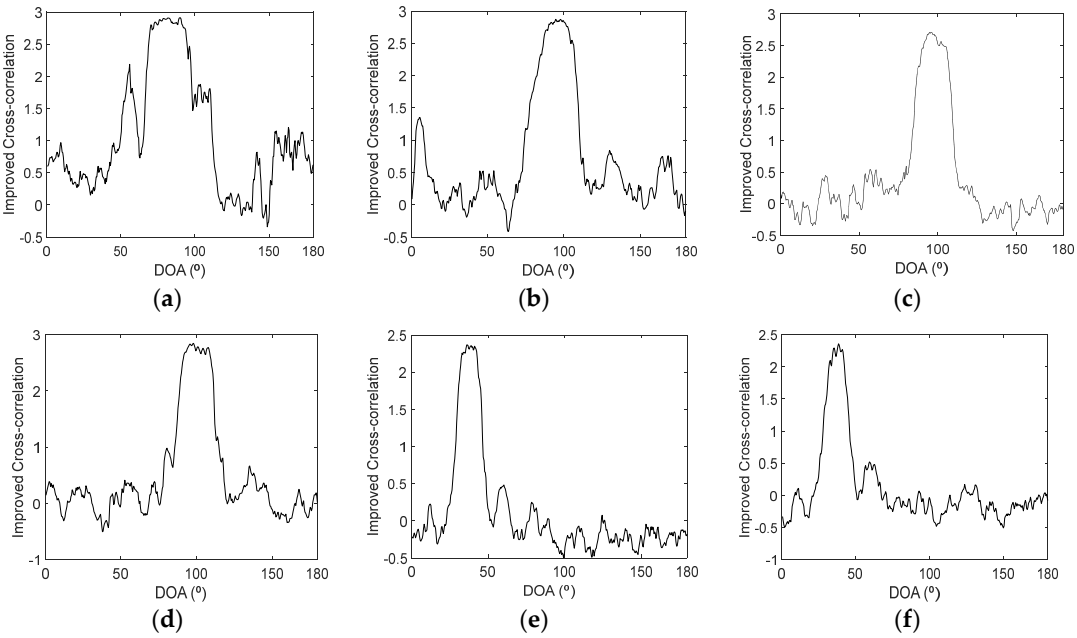

Figure 10. The DOA estimation results using the proposed method outdoors at distances of (**a**) 500 m, (**b**) 1000 m, (**c**) 1500 m, (**d**) 2000 m, (**e**) 2500 m, and (**f**) 3000 m.

Parameter estimation for low-altitude signal sources has not yet been considered in the literature. Thus, two common parameter estimation methods are employed here for comparison with the proposed algorithm. The results with the HOC method [29] for different outdoor distances are given in Figure 11. The position of the maximum value is used as the frequency estimate and the DOA. The estimation accuracy is very poor for distances greater than 1500 m. Figure 12 gives the results for the CFAR method [28] at different outdoor distances and shows that the performance with this method is poor for long distances.

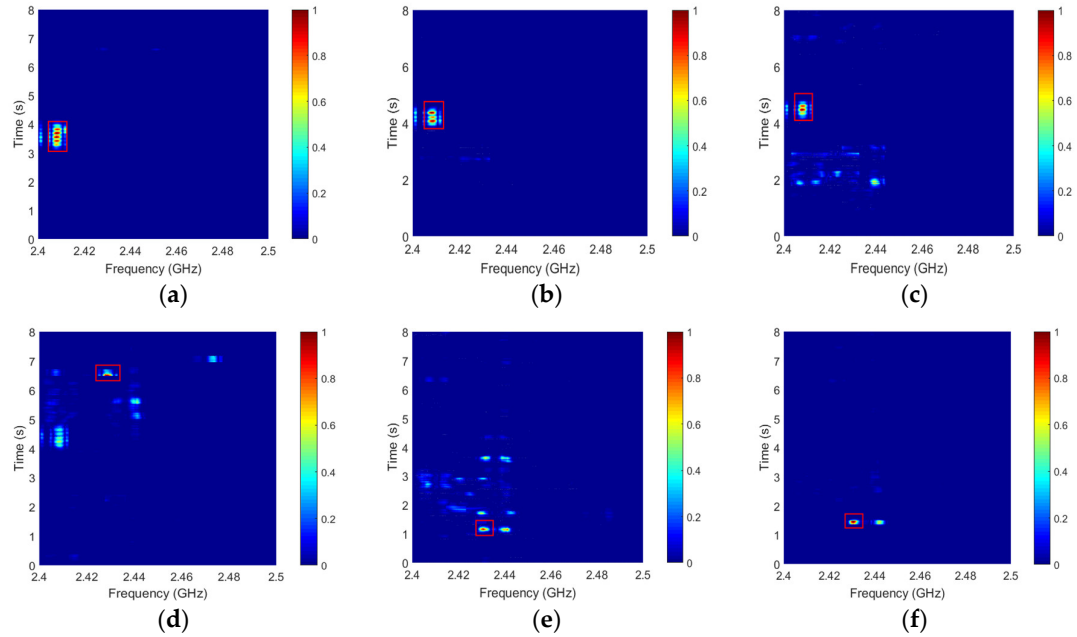

Figure 11. The results for the higher-order cumulant (HOC) method outdoors at distances of (**a**) 500 m, (**b**) 1000 m, (**c**) 1500 m, (**d**) 2000 m, (**e**) 2500 m, and (**f**) 3000 m.

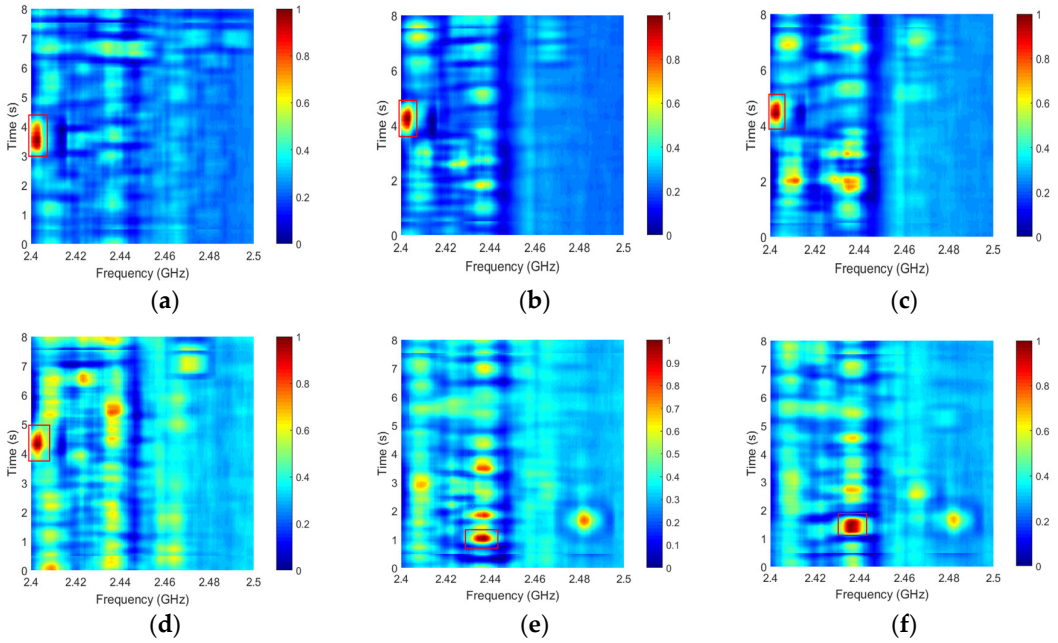

Figure 12. The results for the constant false alarm rate (CFAR) method outdoors at distances of (**a**) 500 m, (**b**) 1000 m, (**c**) 1500 m, (**d**) 2000 m, (**e**) 2500 m, and (**f**) 3000 m.

The estimated frequency, direction of arrival, distance, SNR, and maximum improved cross-correlation for the proposed method are given in Table 1. The maximum cross-correlation without a UAV present is much lower than when a UAV is present. When the UAV is present, the maximum cross-correlation and SNR decrease with distance. The reference distance for distance estimation is 500 m. These results show that the difference between the estimated and actual distances increases with distance. Table 2 shows the corresponding parameter estimation errors for the proposed, HOC, and CFAR methods. These results indicate that the proposed method provides better performance, particularly at long distances.

Table 1. Estimated parameters with the proposed method in an outdoor environment. UAV: unmanned aerial vehicle; R_{jk}: improved cross-correlation matrix; f_{start}: the start of the UAV signal; f_{range}: the range of the UAV signal; $\dot{p}$: estimated direction of arrival; d: the distance between the source and receiver; SNR: signal-to-noise ratio.

Distance between Rx and c (m)	UAV Present						UAV Not Present
	Max R_{jk}	f_{start} (GHz)	f_{range} (GHz)	$\dot{p}$ (°)	d (m)	SNR	Max R_{jk}
500	2.907	2.401776	0.00954	90.22	512.56	0.6634	1.381
1000	2.87	2.401746	0.00953	94.58	986.27	0.4901	1.469
1500	2.84	2.401764	0.00955	96.09	1520.38	0.2940	1.149
2000	2.708	2.401782	0.00951	97.83	1972.53	0.2216	1.32
2500	2.352	2.471985	0.00953	36.43	2531.74	0.1649	1.647
3000	2.295	2.471981	0.00954	38.35	3040.13	0.1083	1.285

Table 2. Parameter estimation errors for UAV detection using three methods in an outdoor environment. CFAR: constant false alarm rate; HOC: higher-order cumulant.

Method		500 m	1000 m	1500 m	2000 m	2500 m	3000 m
CFAR	Error (MHz)	0.621	0.815	1.049	1.347	38.752	39.891
	Error (°)	7.02	0.878	2.16	2.588	13.793	5.198
HOC	Error (MHz)	5.751	6.631	6.035	25.937	41.590	41.713
	Error (°)	6.143	3.015	0.855	47.07	11.205	4.478
Proposed	Error (MHz)	0.018	0.012	0.006	0.024	0.007	0.011
	Error (°)	4.405	0.618	2.18	1.6	0.605	0.708

4.1.2. Outdoor Passive Detection of Multiple Low-Altitude Signal Sources

In order to evaluate the ability of the proposed method to detect multiple UAVs simultaneously, the outdoor experiment was repeated using two Phantom 4 Pro UAVs, $u1$ and $u2$. The UAVs hovered at the same distance, but with different angles. The normalized time–frequency diagrams after filtering are shown in Figure 13 for different outdoor distances between the UAVs and receiver. For distances of 500 m, 1500 m, and 2500 m, the actual directions of the arrival and start frequencies of $u1$ were 97.905°, 2.421484 GHz; 112.52°, 2.421484 GHz; and 80.55°, 2.421484 GHz, respectively. The actual directions of the arrival and start frequencies of $u2$ were 124.92°, 2.471758 GHz; 47.71°, 2.471758 GHz; and 130.05°, 2.471758 GHz for the same distances of 500 m, 1500 m, and 2500 m, respectively.

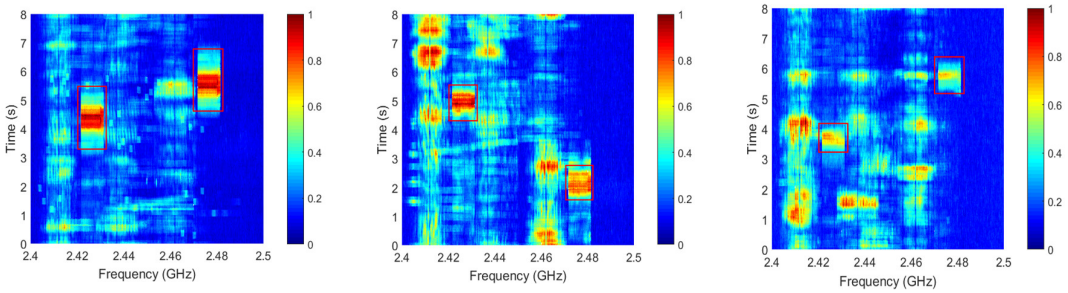

Figure 13. Normalized time–frequency diagrams after filtering for two UAVs outdoors at distances of (**a**) 500 m, (**b**) 1500 m, and (**c**) 2500 m.

The results for the improved cross-correlation method at different outdoor distances are shown in Figure 14 and indicate that two UAVs can be simultaneously detected successfully. The DOA and start frequency estimates for $u1$ were 98.347°, 2.421445 GHz; 113.242°, 2.421426 GHz; and 79.402°, 2.421436 GHz for distances of 500 m, 1500 m, and 2500 m, respectively. The DOA and start frequency estimates for $u2$ were 125.865°, 2.471701 GHz; 48.263°, 2.471680 GHz; and 129.465°, 2.471802 GHz for distances of 500 m, 1500 m, and 2500 m, respectively. The corresponding performance with the HOC and CFAR methods is shown in Figures 15 and 16, respectively. Table 3 shows the outdoor parameter estimation errors for the two UAVs using the three methods. For $u1$, the frequency errors were 0.039 MHz, 3.613 MHz, and 2.732 MHz at a distance of 500 m for the proposed, HOC, and CFAR algorithms, respectively. For all distances, the DOA estimation error was within 3° using the proposed method. This indicates that this method is able to accurately detect multiple low-altitude signal sources.

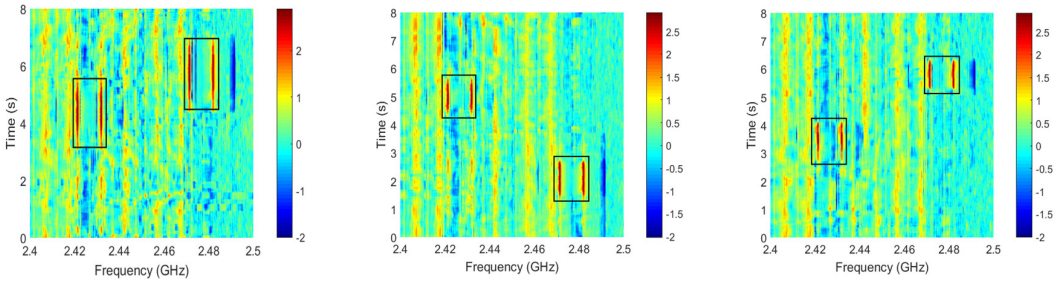

Figure 14. The results for the improved cross-correlation method for two UAVs outdoors at distances of (**a**) 500 m, (**b**) 1500 m, and (**c**) 2500 m.

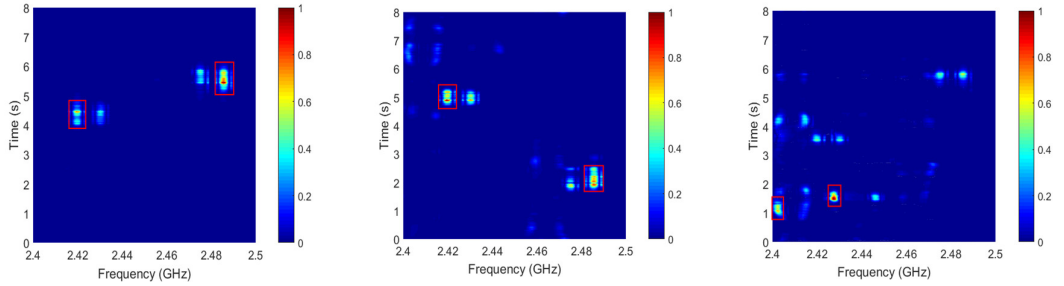

Figure 15. The results for the HOC method with two UAVs outdoors at distances of (**a**) 500 m, (**b**) 1500 m, and (**c**) 2500 m.

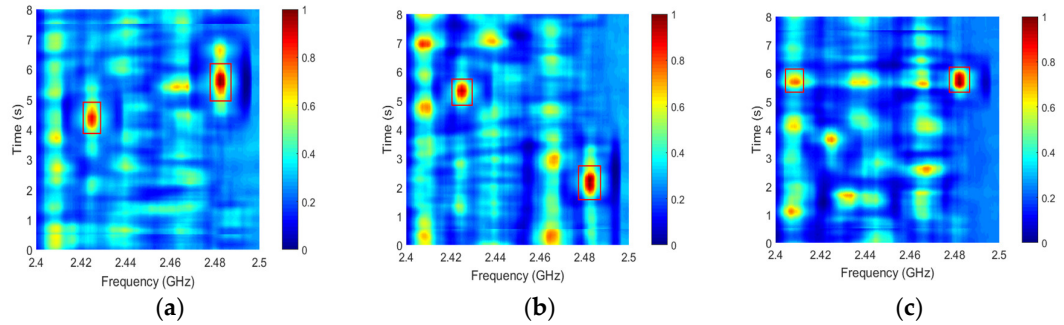

Figure 16. The results for the CFAR method for two UAVs outdoors at distances of (**a**) 500 m, (**b**) 1500 m, and (**c**) 2500 m.

Table 3. Parameter estimation errors for two UAVs using three methods in an outdoor environment.

Method		500 m		1500 m		2500 m	
		***u*1**	***u*2**	***u*1**	***u*2**	***u*1**	***u*2**
CFAR	Error (MHz)	2.732	0.605	0.489	5.450	13.67	0.061
	Error (°)	1.050	2.250	1.430	1.550	47.71	2.520
HOC	Error (MHz)	3.613	5.781	3.711	5.924	19.04	47.05
	Error (°)	2.400	1.330	2.270	4.960	57.15	95.78
Proposed	Error (MHz)	0.039	0.057	0.058	0.078	0.049	0.044
	Error (°)	0.442	1.045	1.122	0.553	1.148	0.585

4.2. Indoor Experiment

The indoor passive detection performance of single and multiple low-altitude signal sources is evaluated in this section. Two methods are used to analyze the false alarm probability and

missing alarm probability, and a comparison of three algorithms for indoor parameter estimation is also presented.

4.2.1. Indoor Passive Detection of a Low-Altitude Signal Source

The indoor data was obtained in a research laboratory with dimensions 10 m × 15 m × 5 m using a Phantom 4 Pro UAV. The normalized time–frequency diagrams after filtering are shown in Figure 17 for distances of 5 m and 10 m between the UAV and receiver. For these distances, the actual directions of the arrival and start frequencies were 117.60°, 2.401758 GHz; and 98.67°, 2.401758 GHz.

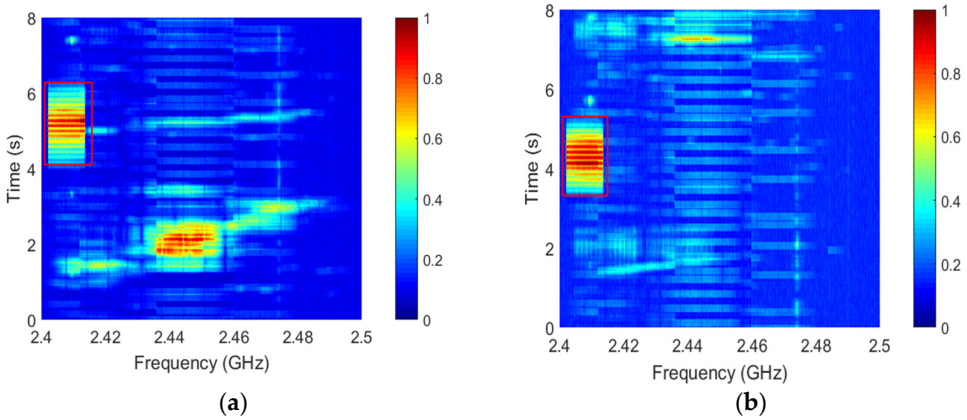

Figure 17. Normalized time–frequency diagrams after filtering at indoor distances of (**a**) 5 m and (**b**) 10 m.

Figure 18 presents the false alarm probability and missing alarm probability for different numbers of datasets and indoor distances. For the AM and improved cross-correlation threshold classification method, the false alarm probabilities for 1000 datasets were 0.09 and 0.0621, respectively. With 1000 datasets and a distance of 5 m, the missing alarm probabilities were 0.0542 and 0.0171 for the AM and proposed method, respectively, as shown in Figure 18b. These results indicate that the proposed method provides better performance.

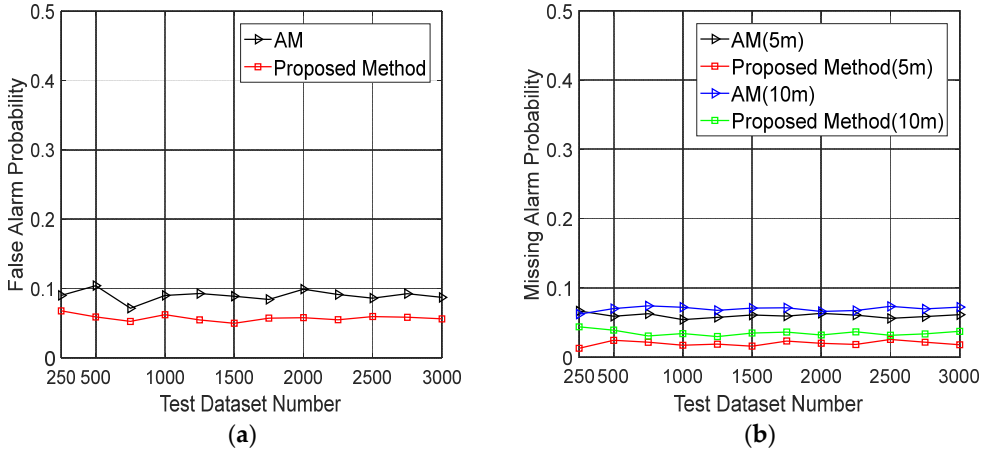

Figure 18. (**a**) The false alarm probability with different numbers of indoor datasets, and (**b**) the missing alarm probability with different numbers of indoor datasets and two distances.

The results for the improved cross-correlation method at different indoor distances are given in Figure 19. This shows that the cross-correlation values are greater in the target area compared to where there is only clutter and noise. Figures 20 and 21 present the frequency and DOA estimation results using the proposed method, respectively. The frequency estimates are 2.401737 GHz and 2.401741 GHz

and the DOA estimates are 117.13° and 99.92° for distances of 5 m and 10 m, respectively. The results for the HOC and CFAR algorithms at different indoor distances are shown in Figures 22 and 23, respectively. Table 4 gives the indoor parameter estimates for the proposed, HOC, and CFAR methods. These results indicate that the proposed algorithm provides the best performance.

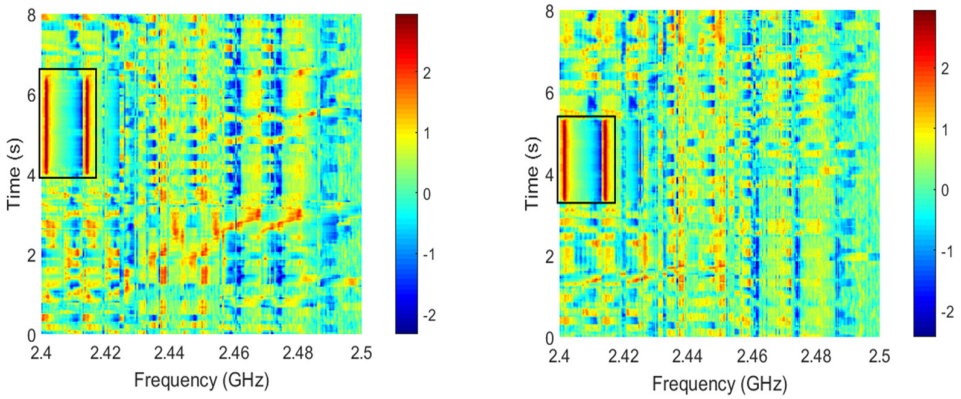

Figure 19. The results for the improved cross-correlation method indoors at distances of (**a**) 5 m and (**b**) 10 m.

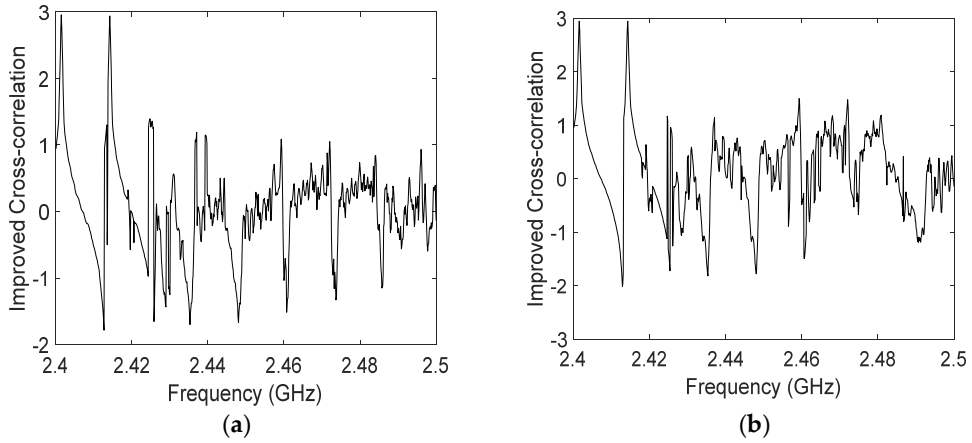

Figure 20. The frequency estimation using the proposed method indoors at distances of (**a**) 5 m and (**b**) 10 m.

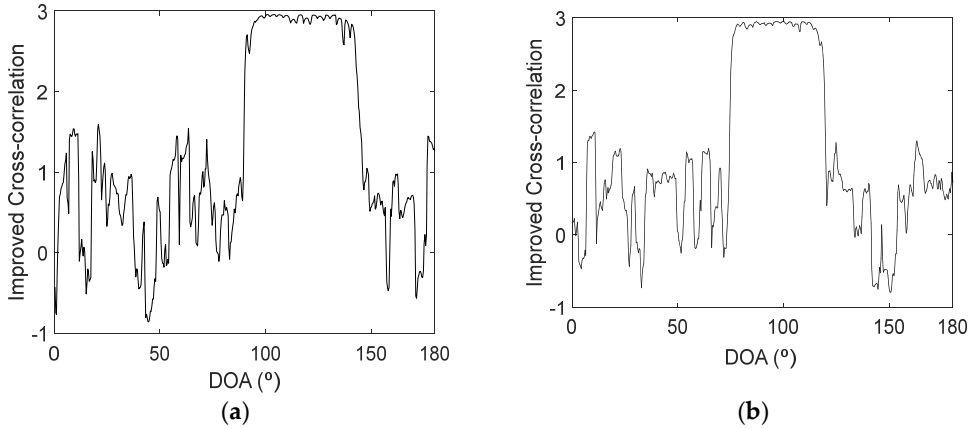

Figure 21. The DOA estimation using the proposed method indoors at distances of (**a**) 5 m and (**b**) 10 m.

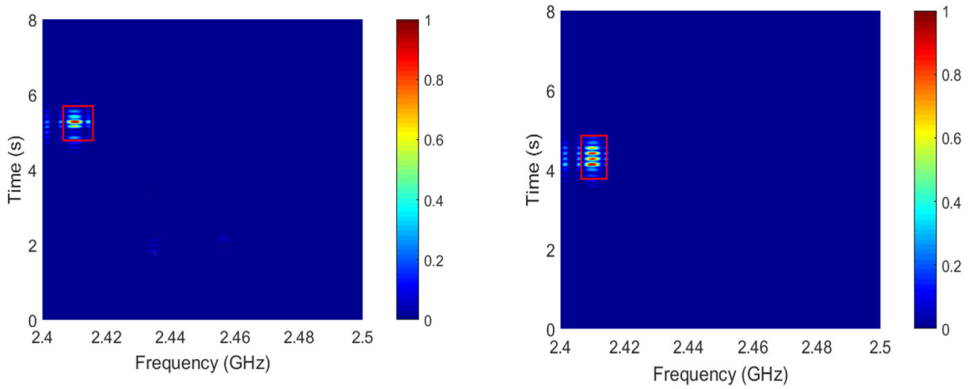

Figure 22. The results for the HOC method indoors at distances of (**a**) 5 m and (**b**) 10 m.

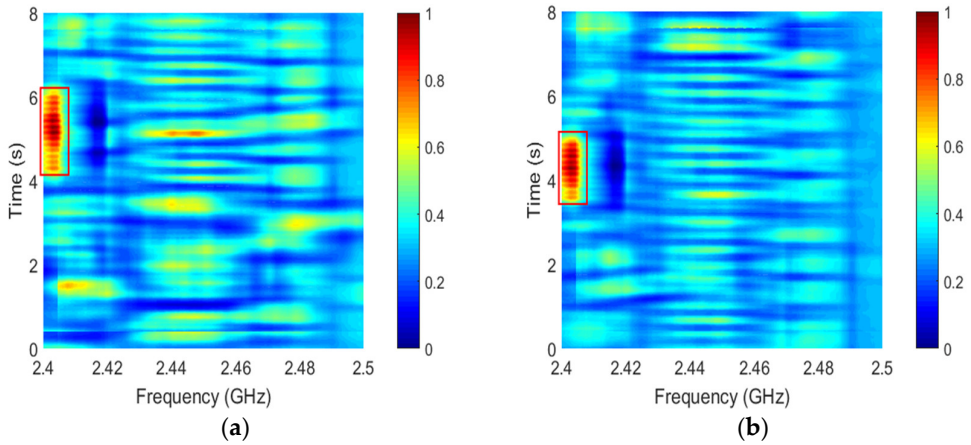

Figure 23. The result for the CFAR method indoors at distances of (**a**) 5 m and (**b**) 10 m.

Table 4. Parameter estimation errors for UAV detection using three methods in an indoor environment.

Method		CFAR	HOC	Proposed
5 m	Error (MHz)	1.324	7.133	0.021
	Error (°)	1.792	0.728	0.470
10 m	Error (MHz)	1.215	6.264	0.017
	Error (°)	2.212	5.452	1.250

4.2.2. Indoor Passive Detection of Multiple Low-Altitude Signal Sources

The indoor experiment was repeated using two Phantom 4 Pro UAVs, $u1$ and $u2$. They were placed on a table at the same distance from the Rx, but with different angles. Figure 24 shows the normalized time–frequency diagrams after filtering for distances of 5 m and 10 m. The actual directions of the arrival and start frequencies of $u1$ were 88.65°, 2.401719 GHz and 78.35°, 2.401719 GHz, and for $u2$, were 105.75°, 2.471719 GHz and 72.45°, 2.471719 GHz at distances of 5 m and 10 m, respectively.

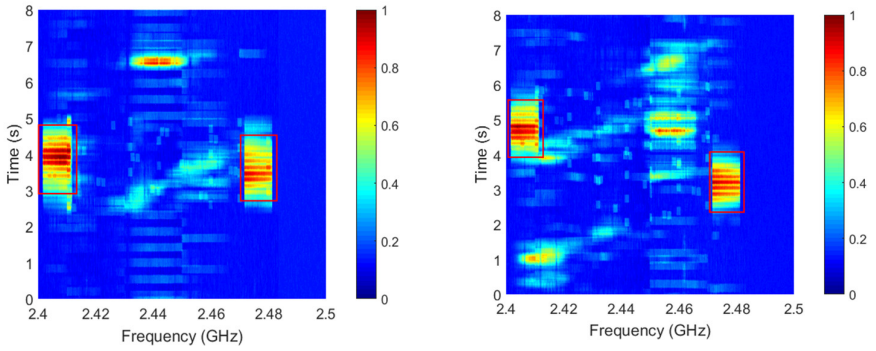

Figure 24. Normalized time–frequency diagrams after filtering for two UAVs indoors at distances of (**a**) 5 m and (**b**) 10 m.

The results for the improved cross-correlation method for the two UAVs are shown in Figure 25. The frequency and DOA estimates were 2.401667 GHz, 86.67° and 2.401741 GHz, 79.81° for $u1$ at distances of 5 m and 10 m, respectively. The corresponding values for $u2$ were 2.471628 GHz, 107.91° and 2.471671 GHz, 73.48°. The corresponding results for the HOC and CFAR methods are shown in Figures 26 and 27, respectively. Table 5 gives the parameter estimation errors for the three methods. These results indicate that the proposed algorithm again provides the best performance.

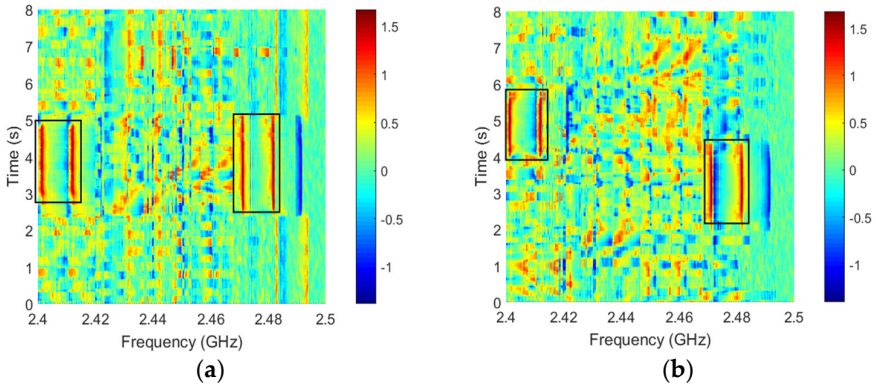

Figure 25. The results for the improved cross-correlation method for two UAVs indoors at distances of (**a**) 5 m and (**b**) 10 m.

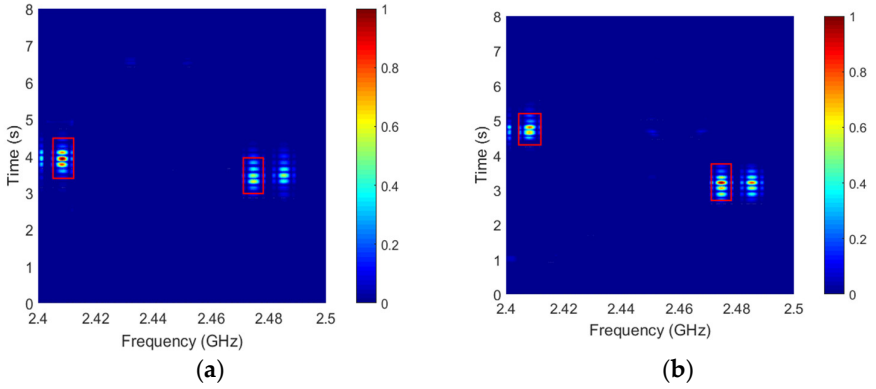

Figure 26. The HOC method results for two UAVs indoors at distances of (**a**) 5 m and (**b**) 10 m.

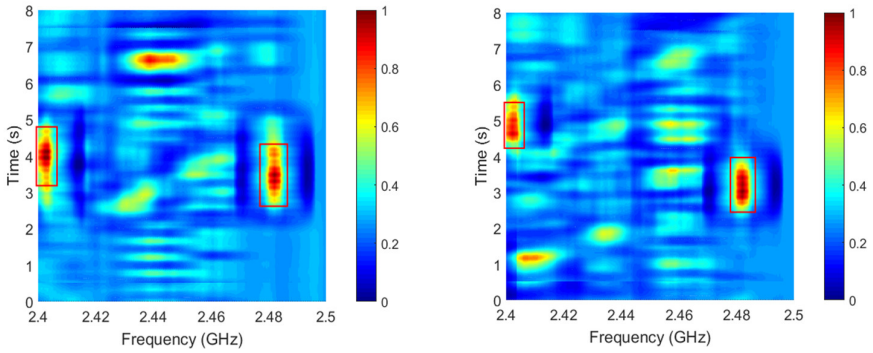

Figure 27. The CFAR method results for two UAVs indoors at distances of (**a**) 5 m and (**b**) 10 m.

Table 5. Parameter estimation errors for two UAVs using three methods in an indoor environment.

Method		5 m		10 m	
		***u*1**	***u*2**	***u*1**	***u*2**
CFAR	Error (MHz)	0.625	0.351	0.332	0.254
	Error (°)	3.20	1.43	2.73	4.59
HOC	Error (MHz)	6.00	3.95	5.70	3.85
	Error (°)	1.35	4.10	2.73	1.80
Proposed	Error (MHz)	0.052	0.091	0.022	0.048
	Error (°)	1.98	2.16	1.46	1.03

5. Conclusions

Passive detection of low-altitude signal sources was proposed using an improved cross-correlation algorithm. The DOA and communication frequency estimation of these signals was studied. An algorithm was developed to estimate the SNR and the distance between the signal source and receiver. A UAV was considered in the experiments as a typical low-altitude signal source. The results obtained show that the proposed method has a low false alarm probability as well as a low missed alarm probability. UAV parameters such as communication frequency, DOA, distance, and SNR were estimated accurately in both outdoor and indoor environments using this method. In addition, the proposed algorithm provides better performance than several well-known passive detection algorithms in the literature. Thus, the proposed method is more suitable for the long-distance passive detection of low-altitude signal sources.

Author Contributions: C.C. conceived and designed the passive detection algorithm, implemented the experiments, and analyzed the data; H.Y., H.Z., Y.W., and T.A.G. provided comments on the paper organization, contributed towards the performance results and evaluation, and were involved in writing the manuscript.

Funding: This work was supported by the National Natural Science Foundation of China (61871354, 6172780176, 61701462, 61727806, and 41527901), the Qingdao National Laboratory for Marine Science and Technology (2017ASKJ01), the Qingdao Science and Technology Plan (17-1-1-7-jch), the Nature Science Foundation of Shandong Province (ZR2017MD027), and the Fundamental Research Funds for the Central Universities (201713018).

Conflicts of Interest: The authors declare no conflicts of interest.

References

1. Itkin, M.; Kim, M.; Park, Y. Development of Cloud-Based UAV Monitoring and Management System. *Sensors* **2016**, *16*, 1913. [CrossRef] [PubMed]
2. Zhang, H.; Cao, C.H.; Xu, L.W.; Gulliver, T.A. A UAV Detection Algorithm Based on an Artificial Neural Network. *IEEE Access* **2018**, *6*, 24720–24728. [CrossRef]

3. Wiggerich, B.; Wiggerich, B.; Pfingsthorn, M. Safety, Security, and Rescue Missions with an Unmanned Aerial Vehicle (UAV). *J. Intell. Robot. Syst.* **2011**, *64*, 57–76.
4. Bhardwaj, A.; Sam, L.; Akanksha, J.; Martin-Torres, F.; Kumar, R. UAVs as Remote Sensing Platform in Glaciology: Present Applications and Future Prospects. *Remote Sens. Environ.* **2016**, *175*, 196–204. [CrossRef]
5. Petritoli, E.; Leccese, F. Improvement of Altitude Precision in Indoor and Urban Canyon Navigation for Small Flying Vehicles. In Proceedings of the IEEE Metrology for Aerospace, Benevento, Italy, 4–5 June 2015; pp. 56–60.
6. Kopáčik, A.; Kajánek, P.; Lipták, I. Systematic Error Elimination Using Additive Measurements and Combination of Two Low Cost IMSs. *IEEE Sens. J.* **2016**, *16*, 6239–6248. [CrossRef]
7. Unlu, E.; Zenou, E.; Riviere, N. Generic Fourier Descriptors for Autonomous UAV Detection. In Proceedings of the International Conference on Pattern Recognition Applications and Methods, Funchal, Madeira, Portugal, 16–18 January 2018; pp. 550–554.
8. Ren, J.; Jiang, X. Regularized 2-D Complex-log Spectral Analysis and Subspace Reliability Analysis of Micro-Doppler Signature for UAV Detection. *Pattern Recognit.* **2017**, *69*, 225–237. [CrossRef]
9. Hu, Q.W.; Wang, S.H.; Fu, C.W.; Ai, M.Y.; Yu, D.B.; Wang, W.D. Fine Surveying and 3D Modeling Approach for Wooden Ancient Architecture via Multiple Laser Scanner Integration. *Remote Sens.* **2016**, *8*, 270. [CrossRef]
10. Gamba, M.T.; Marucco, G.; Pini, M.; Ugazio, S.; Falletti, E.; Presti, L.L. Prototyping a GNSS-Based Passive Radar for UAVs: An Instrument to Classify the Water Content Feature of Lands. *Sensors* **2015**, *15*, 28287–28313. [CrossRef] [PubMed]
11. Zhao, H.Y.; Liu, J.; Zhang, Z.J.; Liu, H.; Zhou, S. Linear Fusion for Target Detection in Passive Multistatic Radar. *Signal Process.* **2016**, *130*, 175–182. [CrossRef]
12. Noroozi, A.; Sebt, M.A. Target Localization in Multistatic Passive Radar Using SVD Approach for Eliminating the Nuisance Parameters. *IEEE Trans. Aerosp. Electron. Syst.* **2017**, *53*, 1660–1671. [CrossRef]
13. Berdanier, C.; Wicks, M.; Baker, C.; Wu, Z. Phase Based 2D Passive Source Localisation Using Receiver Networks. *IET Radar Sonar Navig.* **2017**, *11*, 2–10. [CrossRef]
14. Radmard, M.; Bayat, S.; Farina, A.; Nayebi, M.M. Catching the High Altitude Invisible by Satellite-based Forward Scatter PCL. *Signal Image Video Process.* **2016**, *11*, 1–8. [CrossRef]
15. Gassier, G.; Chabriel, G.; Barrère, J.; Briolle, F.; Jauffret, C. A Unifying Approach for Disturbance Cancellation and Target Detection in Passive Radar Using OFDM. *IEEE Trans. Signal Process.* **2016**, *64*, 5959–5971. [CrossRef]
16. Guo, Y.; Tharmarasa, R.; Kirubarajan, T.; Wong, S.; Jassemi, R. Passive Coherent Location with Unknown Transmitter States. *IEEE Trans. Aerosp. Electron. Syst.* **2017**, *53*, 148–168. [CrossRef]
17. Lee, K.H.; Chang, J.H.; Kim, N.S.; Kang, S.; Kim, Y. Frequency-Domain Double-Talk Detection Based on the Gaussian Mixture Model. *IEEE Signal Process. Lett.* **2010**, *17*, 453–456. [CrossRef]
18. Zhu, H.; Yu, F. A Cross-Correlation Technique for Vehicle Detections in Wireless Magnetic Sensor Network. *IEEE Sens. J.* **2016**, *16*, 4484–4494. [CrossRef]
19. Su, D.; Luo, J.; Shuang, T.; Tu, Y.; Li, C.; Deng, Z. A Cross Correlation Phase Offset Method Based on Hilbert Transform. In Proceedings of the World Congress on Intelligent Control and Automation, Shenyang, China, 29 June–4 July 2014; pp. 5733–5736.
20. Dodge, D.A.; Harris, D.B. Large-Scale Test of Dynamic Correlation Processors: Implications for Correlation-Based Seismic Pipelines. *Bull. Selsmol. Soc. Am.* **2016**, *106*, 435–452. [CrossRef]
21. Tong, J.; Xie, W.; Hu, Y.H.; Bao, M.; Li, X.; He, W. Estimation of Low-altitude Moving Target Trajectory Using Single Acoustic Array. *J. Acoust. Soc. Am.* **2016**, *139*, 1848–1858. [CrossRef] [PubMed]
22. He, Z.; Fu, L.; Han, W.; Mai, R. Precise Algorithm for Frequency Estimation under Dynamic and Step-change Conditions. *IET Sci. Meas. Technol.* **2015**, *9*, 842–851. [CrossRef]
23. Liang, X.L.; Zhang, H.; Gulliver, T.A.; Fang, G.Y.; Ye, S.B. An Improved Algorithm for Through-wall Target Detection Using Ultrawideband Impulse Radar. *IEEE Access* **2017**, *5*, 22101–22118. [CrossRef]
24. Luo, Q.; Peng, Y.; Peng, X.; Saddik, A.E. Uncertain Data Clustering-Based Distance Estimation in Wireless Sensor Networks. *Sensors* **2014**, *14*, 6584–6605. [CrossRef] [PubMed]
25. Xu, L.W.; Wang, J.J.; Zhang, H.; Gulliver, T.A. Performance Analysis of IAF Relaying Mobile D2D Cooperative Networks. *J. Frankl. Inst.* **2017**, *354*, 902–916. [CrossRef]
26. Lv, X.; Xing, M.; Zhang, S.; Bao, Z. Keystone Transformation of the Wigner-Ville Distribution for Analysis of Multicomponent LFM Signals. *Signal Process.* **2009**, *89*, 791–806. [CrossRef]

27. Bush, D.R.; Xiang, N. Spectrum-dependent Bandpass Beampattern Modeling and Spatial Filtering with Coprime Linear Microphone Arrays. *J. Acoust. Soc. Am.* **2017**, *141*, 3843. [CrossRef]
28. Xu, Y.; Wu, S.; Chen, C.; Chen, J.; Fang, G. A Novel Method for Automatic Detection of Trapped Victims by Ultrawideband Radar. *IEEE Trans. Geosci. Remote Sens.* **2012**, *50*, 3132–3142. [CrossRef]
29. Xu, Y.; Dai, S.; Wu, S.; Chen, J.; Fang, G. Vital Sign Detection Method Based on Multiple Higher Order Cumulant for Ultrawideband Radar. *IEEE Trans. Geosci. Remote Sens.* **2012**, *50*, 1254–1265. [CrossRef]